remote sensing

MDPI

Article

A New Waveform Design Method for Multi-Target Inverse Synthetic Aperture Radar Imaging Based on Orthogonal Frequency Division Multiplexing Chirp

Xuebo Zou, Guanghu Jin *, Feng He and Yongsheng Zhang

College of Electronic Science, National University of Defense Technology, Changsha 410073, China; zouxuebo21@nudt.edu.cn (X.Z.); hefeng@nudt.edu.cn (F.H.); zhangyongsheng@nudt.edu.cn (Y.Z.)
* Correspondence: guanghujin@nudt.edu.cn

Abstract: With the increasing use of the strategy and group target attack method in the modern battlefield, multi-target inverse synthetic aperture radar (ISAR) imaging simultaneously with high efficiency draws more and more attention, which gives a promising prospect for aerospace target detection and recognition in the multi-target scenario. To overcome the shortcomings of traditional multi-target imaging with one beam at one pulse repetition time (PRT) based on phase array radar (PAR), this paper proposes a novel multi-target imaging waveform design method based on the newly full digital array radar (DAR). Firstly, we propose using radar waveform diversity with 2D orthogonality to realize multi-target ISAR imaging with high imaging quality and efficiency. Then, to meet the constant modulus requirement for maximizing the transmitting power, orthogonal frequency division multiplexing (OFDM) chirp theory is proposed to directly generate the transmit waveform instead of the traditional optimization method with the nonconvex problem for waveform design. Based on time-variant weighted and time diversity technology, a of group transmit waveforms is designed, which can form multiple beams simultaneously and make the signals arriving at different targets approximately orthogonal. Finally, simulations and experiments are carried out to demonstrate the effectiveness of the proposed method.

Keywords: multi-target; ISAR imaging; waveform design; OFDM chirp

check for updates

Citation: Zou, X.; Jin, G.; He, F.; Zhang, Y. A New Waveform Design Method for Multi-Target Inverse Synthetic Aperture Radar Imaging Based on Orthogonal Frequency Division Multiplexing Chirp. *Remote Sens.* **2024**, *16*, 308. https://doi.org/10.3390/rs16020308

Academic Editors: Xueru Bai, Li Wang, Tian Tian and Weiwei Fan

Received: 10 November 2023
Revised: 27 December 2023
Accepted: 7 January 2024
Published: 11 January 2024

Copyright: © 2024 by the authors. Licensee MDPI, Basel, Switzerland. This article is an open access article distributed under the terms and conditions of the Creative Commons Attribution (CC BY) license (https://creativecommons.org/licenses/by/4.0/).

1. Introduction

In recent decades, the increase in collaborative attack methods on aerospace targets such as aircraft, missiles and satellites has made the modern battlefield more diverse and complex [1–3], which requires the radar to obtain information from multiple targets simultaneously and efficiently [4–16]. ISAR provides a way to obtain high-resolution images of aerospace targets without limitations imposed by time, weather and environmental factors, playing an important role in space target monitoring, recognition and other fields. Typically, traditional ISAR imaging algorithms can only process one target, as mutual interference among different targets makes it difficult to complete motion compensation for all targets simultaneously. To solve this problem, scholars carried out further research and proposed many solutions.

Currently, the mainstream solutions to the problem of multiple targets in the same radar beam are broadly classified into two categories: simultaneous imaging methods [6,7] and separation imaging methods [8–12]. Chen and Qian [7] used the joint time-frequency transform for instantaneous imaging of multiple targets after uniform motion compensation of the echo signal. Kong et al. used the Hough transform and constructed masks to separate the range profiles of each target one by one [8]. However, this method is only applicable in the case of non-overlap of multi-target envelopes. Bai and Xiao obtained the signals of each target through image segmentation based on coarse images [9,10]. Liu et al. modeled the multi-targets as several separated group targets and used the particle

swarm optimization (PSO) algorithm to estimate their motion parameters. They then performed image extraction for the focused individual target by the improved CLEAN algorithm [11]. Li and Su proposed using the Zhang–Suen thinning method to extract skeletons of overlapped range profiles and then used the Radon transform to estimate the range walk [12]. After isolation in the image domain, the targets can be focused by the Phase Gradient Autofocus (PGA) algorithm. In [13], Zhang et al. proposed to separate echoes of multi-ship targets using the Hough transform with the minimum entropy autofocus method in the image domain. In [14], with an integrated Kalman filter (IKF), a blocked Fourier compensation matrix (BFCM) was proposed to compensate for the translation of multiple targets simultaneously. However, most of the existing multi-target imaging algorithms focus on compensating and imaging each target independently and can only handle the case under specific assumptions about the target's motion.

Moreover, with the ability to change beam direction instantaneously of phased array radar (PAR), scholars propose to achieve multi-target ISAR imaging based on pulse resource allocation [15,16], which exploits a new research direction for multi-target detection and recognition. In this way, radar focuses the energy on one beam and switches the beam to interesting directions one by one, making all targets observed alternately. However, due to the pulse resource allocation, the pulse repetition frequency (PRF) for each target will decrease, weakening the correlation of adjacent pulse profiles. For this reason, the effect of range alignment will be worse, which makes the imaging results defocused.

Unlike PAR, MIMO radar transmits multiple probing signals that may be chosen at will, offering waveform diversity and extra degrees of freedom [17,18]. To obtain better performance in radar detection, tracking, and imaging, scholars formed a beampattern of any type by designing non-orthogonal transmit waveforms, which can be classified into two categories: narrowband waveform design and wideband waveform design. Typically, for multi-target ISAR imaging, we show more interest in wideband waveform design about space-frequency cell processing [19–24]. In [20], an efficient waveform design method is proposed to realize the desired spatial-frequency beampattern by the wideband beampattern formation via the iterative technique (WBFIT). Based on the signal model proposed in [20], Liu constructed a cost function by jointly minimizing the matching errors of the beampattern and power spectral density (PSD) and designed transmit waveforms to image multiple targets under a constant modulus constraint [21]. Using a novel iterative optimization algorithm (IOA), Yu et al. designed a constant transmit waveform to approximate a desired beampattern and achieve the prescribed space-frequency nulling in a space-frequency region of interest [22]. With this algorithm, multi-target echoes can be separated very well at the receiving end. In [23], we also proposed to use a simple alternating iterative optimization algorithm to simplify the process of waveform design for multi-target imaging. Chu et al. established a time-frequency-space joint optimization model with respect to the waveform phase matrix and solved it using the conjugate gradient (CG) method, which can be used in multi-target scenes [24]. However, under the constant modulus constraint, the mathematical models proposed in these methods are both nonconvex optimization problems, which cannot be solved directly. An iterative operation in the solutions to these problems will result in a significant time overhead.

In addition, with the advantages of the phased-MIMO technique, Chen et al. proposed an adaptive resource allocation strategy for multi-target imaging [25]. Zhang et al. also proposed using a time-delay receive array to image multiple targets based on the joint range–angle beamforming algorithm [26]. The Radar network is another solution for multiple-target searching, tracking and imaging [27–29]. However, these imaging systems require higher performance and quantity for radar equipment.

Based on the above analysis, an ideal waveform design for multi-target imaging should consider the following issues:

(i) Radar should form multiple beams, ensuring that each target can be illuminated simultaneously.

(ii) The signals arriving at different targets should share the same bandwidth, avoiding a decrease in range resolution.
(iii) The signals arriving at different targets should be approximately orthogonal, ensuring the separability of target echoes.
(iv) The time cost of generating the transmit waveform should be minimized to satisfy the real-time request for ISAR imaging.

Aiming at the above issues, we propose a novel waveform design method for multi-target ISAR imaging based on newly full DAR. We introduce the concept of 2D orthogonality to realize multi-target imaging, which images different targets with orthogonal signals. According to this property, mixed echoes are separated by matched filtering, which can reduce mutual interference among different echoes. After using time-variant-weighted and time-diversity technology to form multiple beams, we directly generate a 2D orthogonal transmit waveform using OFDM chirp modulation [30], saving a lot of time and computing resources. Simulation and experiments are given to demonstrate the effectiveness of the proposed method.

This paper is organized as follows. In Section 2, we analyze the problem of multi-target imaging. In Section 3, we introduce the principle of waveform design for multi-target imaging and analyze the mathematical model of waveform design method based on nonconvex optimization. In Section 4, we provide detailed steps for generating transmit waveforms based on the proposed method and analyze its characteristics. In Section 5, simulation and experimental data are given to demonstrate the effectiveness of the proposed algorithm. Finally, we provide concluding remarks and possible future research directions.

2. Problem Formulation

Traditional ISAR systems image different targets with the same LFM waveform, which allows the echo to be written as

$$s(t,t_m)=\sum_p\sum_i A_{pi}\exp\left\{j\pi K_r\left[t-\frac{2R_{pi}(t_m)}{c}\right]^2\right\}\exp\left\{-j4\pi f_c\frac{R_{pi}(t_m)}{c}\right\} \tag{1}$$

where $R_{pi}(t_m)$ denotes the instantaneous slant range between the radar and the i-th scattering point on the p-th target, which will vary with slow time t_m. t is the fast time. A_{pi} is the complex amplitude of the scattering point, and K_r is the chirp rate. c is the speed of light, and f_c is the carrier frequency.

After matched filtering, the result of the pulse compression is

$$s(t,t_m)=\sum_p\sum_i A_{pi}T_p\mathrm{sinc}\left\{B\left[t-\frac{2R_{pi}(t_m)}{c}\right]\right\}\exp\left\{-j4\pi f_c\frac{R_{pi}(t_m)}{c}\right\} \tag{2}$$

where T_p and B denote the pulse duration and the bandwidth of the LFM signal, respectively. Using Taylor series approximation, we have

$$R_{pi}(t_m)\approx R_p+y_{pi}+v_pt_m+\frac{1}{2}a_pt_m^2+x_{pi}\omega_pt_m \tag{3}$$

where R_p is the initial range between the p-th target and the radar. v_p, a_p and ω_p are the radial velocity, radial acceleration, and angular velocity of the p-th target relative to the radar. We establish a coordinate system with the target center as the origin and the radar line of sight (RLOS) direction as the y-axis, and the spatial location of scattering points can be written as (x_{pi},y_{pi}).

The target's motion relative to the radar can be divided into translation $v_pt_m+1/2a_pt_m^2$ and rotation $x_{pi}\omega_pt_m$, which must be well compensated before imaging. With a cross-correlation algorithm, the range alignment makes the envelope of the same scattering point located at the same range cell to compensate for the translation component. In Figure 1, we can see the variation of echo before and after range alignment. However, all echoes from

different targets at the same slow time will receive the same compensation, leading to a worse translation of some targets. In Figure 2, echoes from different targets have different translations, which cannot be compensated simultaneously with the range cell migration method.

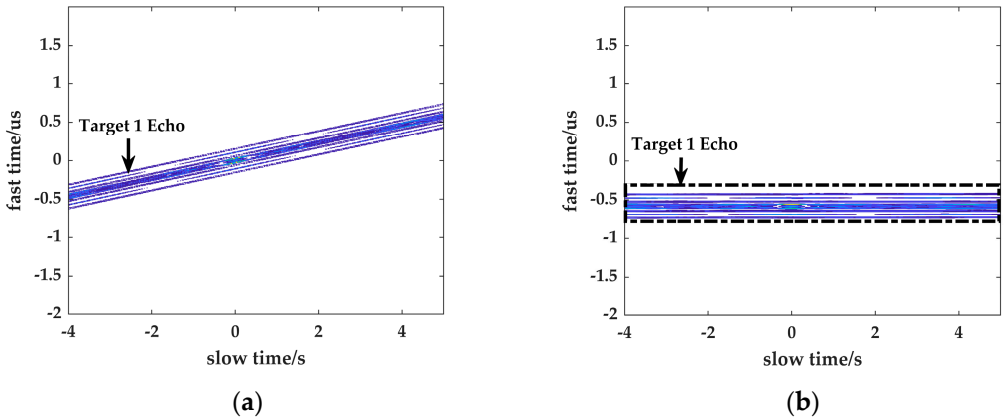


Figure 1. Echo of a single target. (**a**) Raw data; (**b**) range alignment.

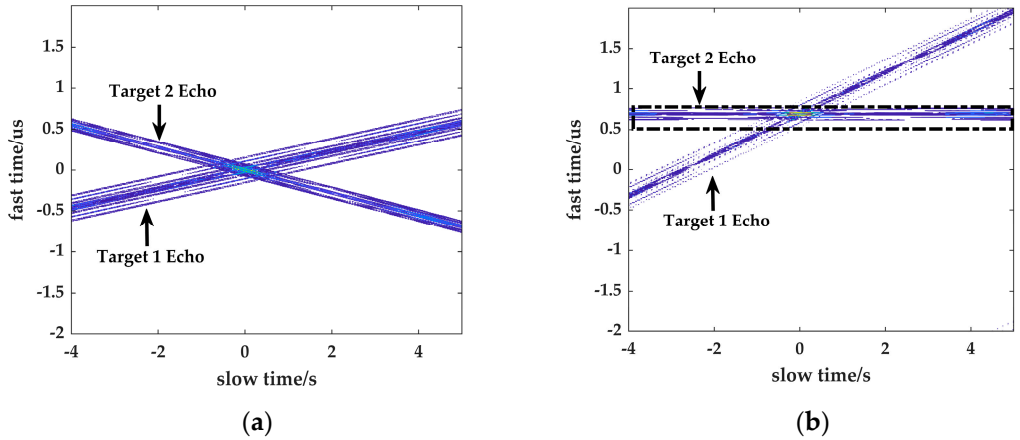


Figure 2. Echoes of multiple targets. (**a**) Raw data; (**b**) range alignment.

PAR adopts the conventional time division multi-beam technology, which allocates the pulse resources to different targets by switching beams to interesting directions one by one. Two ways are given to achieve it, which are shown in Figure 3. The former divides the pulse duration T_p into multiple sub-pulses, and each sub-pulse's waveform can be designed independently. T_{p-h} is the duration of the h-th sub-pulse, and $y_h(t)$ is the synthetic signal corresponding to the h-th sub-pulse's waveform. Obviously, time and bandwidth resources will become tight as the number of targets increases. In the second way, radar only observes one target in one PRT, causing a decrease in the PRF for each target. This change will significantly weaken the correlation of adjacent profiles, making the effect of range alignment worse. For this reason, the imaging results will be defocused.

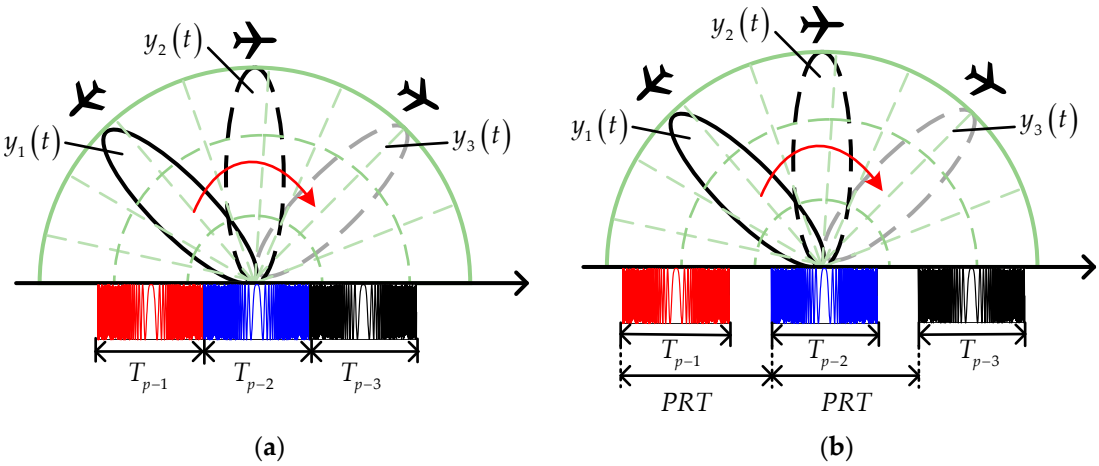


Figure 3. Pulse allocation. (**a**) Intrapulse allocation; (**b**) pulse-to-pulse allocation.

3. Multi-Target ISAR Imaging with 2D Orthogonal Waveform

3.1. Principle of Waveform Design for Multi-Target ISAR Imaging

For the sake of multi-target imaging, it is desirable to concentrate the radiation power in the target direction while lowering the mutual interference between different echoes. To this end, we propose a radar system based on the concept of beam-waveform 2D orthogonality, which is shown in Figure 4.

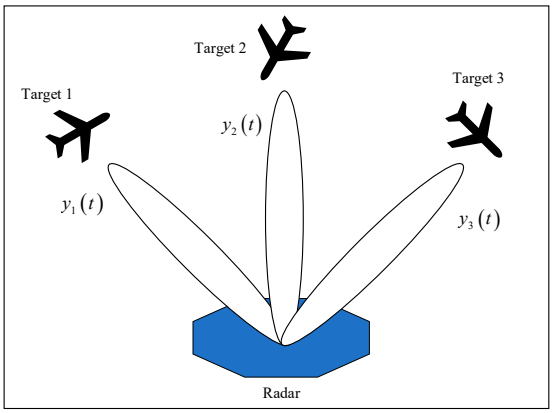


Figure 4. The multi-target ISAR imaging system.

In Figure 4, the radar forms multiple beams pointing to different targets, which focuses the energy on the target region. Synthetic signals $y_h(t)$ are approximately orthogonal to each other, ensuring the separability of multi-target echoes, which can be described as

$$\int_B Y_h(f)Y_j^*(f)df = \begin{cases} c_0, h = j \\ 0, h \neq j \end{cases} \tag{4}$$

where B is the bandwidth and c_0 is a constant. $Y_h(f)$ is the frequency spectrum of the signal $y_h(t)$. However, due to the difference between the time delay of multiple targets, we should set non-overlapping spectrums to satisfy the orthogonality, which is

$$Y_h(f)Y_j^*(f) = 0, h \neq j \tag{5}$$

It is worth noting that the signals $Y_h(f)$ should cover the full bandwidth B, avoiding a decrease in resolution for any target. In addition, to ensure the orthogonality of multi-target

echoes, the frequency spectrum of synthetic signals should not overlap with each other, which can be expressed as

$$\begin{cases} Y_1[p] = \begin{bmatrix} A_1 e^{j\phi_1} & 0 & \cdots & 0 & A_{H+1} e^{j\phi_{H+1}} & 0 & \cdots & 0 & \cdots \end{bmatrix}_{1\times N} \\ Y_2[p] = \begin{bmatrix} 0 & A_2 e^{j\phi_2} & \cdots & 0 & 0 & A_{H+2} e^{j\phi_{H+2}} & \cdots & 0 & \cdots \end{bmatrix}_{1\times N} \\ \qquad\qquad\qquad\qquad\qquad \vdots \\ Y_H[p] = \begin{bmatrix} 0 & 0 & \cdots & A_H e^{j\phi_H} & 0 & 0 & \cdots & A_{2H} e^{j\phi_{2H}} & \cdots \end{bmatrix}_{1\times N} \end{cases} \tag{6}$$

where H denotes the number of beams and $Y_h[p]$ is the discrete frequency spectrum of signal $y_h(t)$. N is the length of the discrete spectrum. A_q and $\phi_q (q = 1, 2, \cdots N)$ denote the amplitude and phase of the q-th frequency spectrum component. The above signals exploit the orthogonality of discrete frequency components, which allows full bandwidth to be used for imaging each target. Assuming the received signal is

$$R(f) = \sum_p Y_p(f) \exp\{-j2\pi f \tau_p\} + N(f) \tag{7}$$

where $N(f)$ denotes the frequency spectrum of random noise, and τ_p is the delay of the p-th target. After matched filtering with the h-th orthogonal signal $Y_h(f)$, the echo can be expressed as follows:

$$\begin{aligned} R_h(f) &= R(f) Y_h^*(f) \\ &= \left[\sum_p Y_p(f) \exp\{-j2\pi f \tau_p\} + N(f) \right] Y_h^*(f) \\ &= |Y_h(f)|^2 \exp\{-j2\pi f \tau_h\} rect\left\{ \frac{f}{B} \right\} + N(f) Y_h^*(f) \end{aligned} \tag{8}$$

Only when $p = h$ is met will there be a target echo in the results. Based on the above analysis, the echo of each target can be obtained separately.

3.2. Waveform Design for Multi-Target Imaging with Non-Convex Optimization Algorithm

As aforementioned, the synthetic signals should satisfy the Formulas (5) and (6), which is difficult to achieve with traditional PAR. The MIMO radar transmits multiple probing waveforms from different antennas, creating a plethora of waveform diversity and extra degrees of freedom to enhance its performance. Based on its advantages, we hope to obtain the 2D orthogonal waveform through the MIMO radar waveform design theory.

Here, we consider a co-located MIMO radar system with M transmit antennas, which are deployed as a uniform linear array (ULA) with inter-element spacing of d. The structure of the array is shown in Figure 5. We assume that the transmit signal of the m-th antenna is

$$s_m(t) = x_m(t) \exp\{j2\pi f_c t\}, 0 \le t \le T_p \tag{9}$$

where $x_m(t)$ denotes the baseband signal of the m-th antenna, f_c denotes the carrier frequency, and T_p denotes the pulse duration. The baseband signal can be sampled as

$$x_m(l) = x_m(t)|_{t=(l-1)T_s}, l = 1, \cdots, L \tag{10}$$

where T_s denotes the sampling interval, l denotes the particular sample number, and $L = T_p / T_s$ denotes the total number of samples. Therefore, the transmit signal can be expressed in matrix form as follows:

$$\mathbf{X} = \begin{bmatrix} x_1(1) & x_1(2) & \cdots & x_1(L) \\ x_2(1) & x_2(2) & \cdots & x_2(L) \\ \vdots & \vdots & \ddots & \vdots \\ x_M(1) & x_M(2) & \cdots & x_M(L) \end{bmatrix} \tag{11}$$

where M denotes the number of antennas. Suppose that the bandwidth of the baseband signal is B, sharing the frequency interval $[-B/2, B/2]$, we define the transformation vector of N-point discrete Fourier transform (DFT) as

$$\mathbf{f}_n = \begin{bmatrix} 1 & \exp\{-j2\pi n/N\} & \cdots & \exp\{-j2\pi(L-1)n/N\} \end{bmatrix}^T \tag{12}$$

where $n = -N/2, \cdots, N/2-1$. We divide the spatial angle interval $[0°, 180°]$ using a grid with points denoted as $\{\theta_k\}_{k=1}^{K}$ and define the transmit steering vector at the frequency $f_c + nB/N$ as

$$\mathbf{a}(n,\theta_k) = \begin{bmatrix} 1 & \exp\left\{j2\pi\left(f_c+\frac{nB}{N}\right)\frac{d\sin\theta_k}{c}\right\} & \cdots & \exp\left\{j2\pi\left(f_c+\frac{nB}{N}\right)\frac{(M-1)d\sin\theta_k}{c}\right\} \end{bmatrix} \tag{13}$$

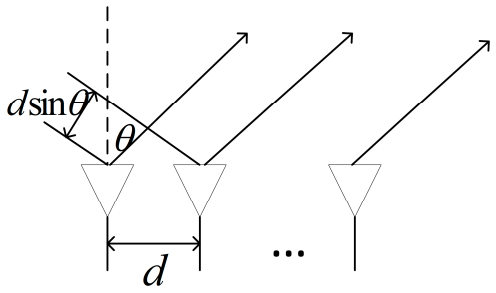


Figure 5. The diagram of the MIMO radar transmit array.

Then, we can obtain the discrete frequency component and power spectrum of the far-field signal arriving at the spatial angle θ_k.

$$\begin{aligned} Y(n,\theta_k) &= \mathbf{a}(n,\theta_k)\mathbf{X}\mathbf{f}_n \\ P(n,\theta_k) &= |Y(n,\theta_k)|^2/N = \mathbf{a}(n,\theta_k)\mathbf{X}\mathbf{f}_n\mathbf{f}_n^H\mathbf{X}^H\mathbf{a}^H(n,\theta_k) \end{aligned} \tag{14}$$

Consequently, the beampattern at the spatial angle θ_k can be defined as

$$G(\theta_k) = \sum_{n=-N/2}^{N/2-1} P(n,\theta_k) \tag{15}$$

Based on the above analysis, we can control the direction of any discrete frequency component and the shape of the beampattern by designing the waveform matrix $\mathbf{X}$. In order to satisfy the concept of the beam-waveform 2D orthogonal, we seek to solve the following matching problem:

$$\min\left\{\sum_{k=1}^{K}[G(\theta_k)-D_k]^2 + \sum_{h=1}^{H}\sum_{n=-N/2}^{N/2-1}[P(n,\theta_k)-d_h]^2\right\} \tag{16}$$

where D_k denotes the desired beampattern, and d_k is the discrete frequency spectrum of the desired synthetic signal in the target direction. This function can be divided into two parts: beampattern matching and discrete frequency spectrum matching. The former forms multiple beams, and the latter guarantees orthogonality of the synthetic signals. However, this is a nonconvex optimization problem because of the constant modulus constraint, which cannot be easily solved.

4. Fast Waveform Design Method for Multi-Target Imaging

4.1. Multi-Beam Forming with Time-Variant Weighting

As mentioned in Section 3, the generation of the 2D orthogonal waveform for multi-target imaging can be divided into two parts under constant modulus constraints. The first step is to form multiple beams simultaneously, which can concentrate the radiation power

in the target direction. Due to the dispersion effect, traditional narrowband beamforming algorithms cannot process wideband signals. Therefore, we plan to solve this problem using the time-variant-weighted algorithm based on a newly full DAR.

Assuming that the baseband transmit signal of the radar is

$$x(t) = \exp\left\{j\pi K_r t^2\right\}, 0 \le t \le T_p \tag{17}$$

where K_r denotes the chirp rate, and T_p denotes the pulse duration. The synthetic signal in the direction θ can be expressed as

$$\begin{aligned} y(t,\theta) &= \sum_{m=1}^{M} \exp\left\{j\pi K_r\left[t-(m-1)\tfrac{d\sin\theta}{c}\right]^2\right\}\cdot\exp\left\{j2\pi f_c\left[t-(m-1)\tfrac{d\sin\theta}{c}\right]\right\} \\ &= \sum_{m=1}^{M} \exp\{j\pi K_r t^2\}\cdot\exp\{j2\pi f_c t\}\cdot\exp\left\{-j2\pi\left(K_r t\tau_m - \tfrac{1}{2}K_r\tau_m^2 + f_c\tau_m\right)\right\} \end{aligned} \tag{18}$$

where f_c denotes the carrier frequency, and $\tau_m = (m-1)d\sin\theta/c$ denotes the delay of the m-th antenna relative to the reference antenna. Thus, the compensation function for the m-th antenna is

$$h_m(\theta,t) = \exp\left\{j2\pi\left(K_r t\tau_m - \frac{1}{2}K_r\tau_m^2 + f_c\tau_m\right)\right\} \tag{19}$$

This is a time-variant function, and the compensation effect makes the transmit signals of different antennas stacked in phase in the direction θ. Therefore, the transmit signals can be written as

$$\widetilde{x}_m(\theta,t) = x(t)\cdot h_m(\theta,t) = \exp\left\{j2\pi\left(\frac{K_r}{2}t^2 + K_r t\tau_m - \frac{1}{2}K_r\tau_m^2 + f_c\tau_m\right)\right\} \tag{20}$$

To form multiple beams simultaneously, we set the transmit signal as

$$w_m(t) = [\widetilde{x}_m(\theta_1,t), \widetilde{x}_m(\theta_2,t), \cdots, \widetilde{x}_m(\theta_H,t)] \tag{21}$$

where H denotes the number of beams. Time duration T_h of each transmit sub-signal can be set to specific values, which makes beampattern gain various in different target directions. However, synthetic signals are not orthogonal to each other, which requires additional processes to separate different targets.

4.2. Orthogonal Waveform Generation with OFDM Modulation Based on Single DAR

The second step of the transmit waveform generation is to make the synthetic signals in target directions orthogonal to each other, ensuring the separability of echoes. In Formula (5), we propose to exploit the orthogonality of discrete frequency components, avoiding a decrease in resolution for any target. To this end, we consider using the OFDM modulation theory, which is used to generate multiple orthogonal waveforms.

Assume the input sequence $s[n]$ with N points sampling length and it can be written as

$$s[n] = \exp\left\{j\pi K_r(nT_s)^2\right\}, n = 0,1,2,\cdots,N-1 \tag{22}$$

where K_r denotes the chirp rate, and T_s denotes the sampling interval. Then, we can obtain its discrete frequency spectrum $S[\overline{p}]$ after DFT as

$$S[\overline{p}] = \mathcal{F}\{s[n]\}, \overline{p} = 0,1,2,\cdots N-1 \tag{23}$$

where $\mathcal{F}\{\cdot\}$ denotes the DFT operator. Based on its discrete frequency spectrum, we can generate two signals through zero interleaving and shift as follows:

$$\begin{aligned} S_1[p] &= \begin{bmatrix} S[0] & 0 & S[1] & 0 & \cdots & S[N-1] & 0 \end{bmatrix} \\ S_2[p] &= \begin{bmatrix} 0 & S[0] & 0 & S[1] & \cdots & 0 & S[N-1] \end{bmatrix} \end{aligned}, p = 0,1,2,\cdots,2N-1 \tag{24}$$

Both signals have $2N$ frequency components and occupy the same bandwidth. It is easy to see their orthogonality through the discrete frequency spectrum. The diagram of the above process is shown in Figure 6.

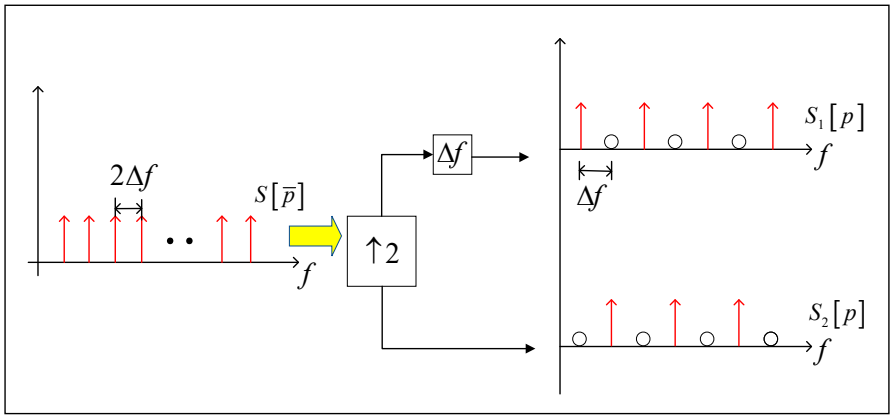


Figure 6. The diagram of the generation of two orthogonal OFDM chirp waveforms.

Since the even components of $S_1[p]$ are zero, the $2N$ point inverse discrete Fourier transform (IDFT) of it can be written as

$$\begin{aligned} s_1[n] &= \sum_{p=0}^{2N-1} S_1[p] \exp\{j2\pi \tfrac{p}{2N} n\} \\ &= \sum_{\overline{p}=0}^{N-1} S[\overline{p}] \exp\left\{j2\pi \tfrac{\overline{p}}{N} n\right\} \\ &= s[n] \cdot rect\left[\tfrac{n}{N}\right] + s[n-N] \cdot rect\left[\tfrac{n-N}{N}\right] \end{aligned} \tag{25}$$

where $n = 0, 1, 2, \cdots, 2N-1$. And the IDFT of $S_2[p]$ is equal to the result of signal $s_1[n]$ after a frequency shift of $\Delta f = F_s/2N$, where F_s denotes the sampling frequency.

Therefore, $s_2[n]$ can be written as

$$\begin{aligned} s_2[n] &= s_1[n] \cdot \exp\left\{j2\pi \Delta f \tfrac{n}{F_s}\right\} \\ &= s_1[n] \cdot \exp\left\{j2\pi \tfrac{F_s}{2N} \tfrac{n}{F_s}\right\} \\ &= s_1[n] \cdot \exp\{j\tfrac{\pi}{N} n\} \end{aligned} \tag{26}$$

In addition, formulas for generating more orthogonal signals can be summarized, and the results are

$$\begin{aligned} s_1[n] &= \sum_{h=1}^{H} s[n-(h-1)N] \cdot rect\left[\tfrac{n-(h-1)N}{N}\right] \\ &\vdots \\ s_H[n] &= s_1[n] \cdot \exp\left\{j\tfrac{2\pi(H-1)n}{HN}\right\} \end{aligned} \tag{27}$$

where $n = 0, 1, 2, \cdots, HN-1$ and H denote the number of orthogonal signals. Typically, scholars use multiple transmitters to emit these orthogonal signals to different regions, which requires multiple radars to be used in the system. In the previous section, we obtained combined signals by time division, and this technology can also be used in OFDM modulation. Letting F_s denote the sampling frequency, we decompose and rewrite the transmit signal in Formula (20) as

$$\begin{cases} w_{\theta_1}[n] = \begin{bmatrix} \widetilde{x}_m(\theta_1, n) & z[n]_{1\times N_2} & \cdots & z[n]_{1\times N_H} \end{bmatrix} \\ w_{\theta_2}[n] = \begin{bmatrix} z[n]_{1\times N_1} & \widetilde{x}_m(\theta_2, n) & \cdots & z[n]_{1\times N_H} \end{bmatrix} \\ \vdots \\ w_{\theta_H}[n] = \begin{bmatrix} z[n]_{1\times N_1} & z[n]_{1\times N_2} & \cdots & \widetilde{x}_m(\theta_H, n) \end{bmatrix} \end{cases} \tag{28}$$

where $N_h = F_s T_h$ denotes the number of sampling points for sub-signal $\widetilde{x}_m(\theta_h, t)$, and $z[n]_{1\times N_h} = \begin{bmatrix} 0 & \cdots & 0 & 0 \end{bmatrix}_{1\times N_h}$ is zero signal. After OFDM modulation, we have

$$\begin{cases} g_1[n] = \begin{bmatrix} w_{\theta_1}[n] & w_{\theta_1}[n] & \cdots & w_{\theta_1}[n] \end{bmatrix} \\ \vdots \\ g_H[n] = \begin{bmatrix} w_{\theta_H}[n] & w_{\theta_H}[n] & \cdots & w_{\theta_H}[n] \end{bmatrix} \cdot \exp\left\{ j\frac{2\pi(H-1)n}{HN} \right\} \end{cases} \tag{29}$$

We let $W_{\theta_h}[p]$ denote the discrete frequency spectrum of $w_{\theta_h}[n]$, and the discrete frequency spectrum of the orthogonal signal $g_h[n]$ is given by

$$\begin{cases} G_1[\widetilde{p}] = \begin{bmatrix} W_{\theta_1}[0] & 0 & \cdots & 0 & W_{\theta_1}[1] & 0 & \cdots & 0 & \cdots & W_{\theta_1}[N-1] & 0 & \cdots & 0 \end{bmatrix} \\ G_2[\widetilde{p}] = \begin{bmatrix} 0 & W_{\theta_2}[0] & \cdots & 0 & 0 & W_{\theta_2}[1] & \cdots & 0 & \cdots & 0 & W_{\theta_2}[N-1] & \cdots & 0 \end{bmatrix} \\ \vdots \\ G_H[\widetilde{p}] = \begin{bmatrix} 0 & 0 & \cdots & W_{\theta_H}[0] & 0 & 0 & \cdots & W_{\theta_H}[1] & \cdots & 0 & 0 & \cdots & W_{\theta_H}[N-1] \end{bmatrix} \end{cases} \tag{30}$$

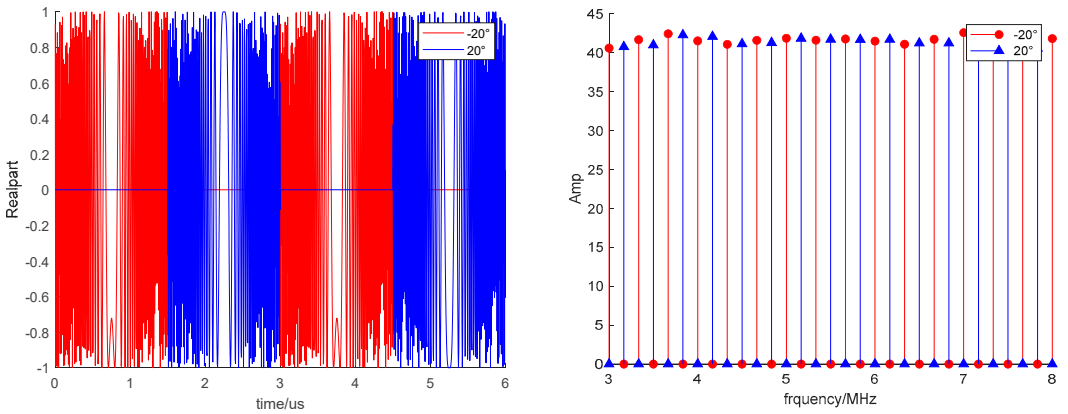
With the above transmit waveforms, the radar emits orthogonal signals in different target directions, requiring multiple transmitters. By utilizing the linear property of the Fourier transform, the sum of time domain signals is equal to the sum of frequency domain signals. Due to the use of time division, the sum of the above signals is still a constant modulus signal, which is

$$g_o[n] = \sum_{h=1}^{H} g_h[n] \tag{31}$$

This transmit waveform can form multiple beams, and OFDM modulation makes the synthetic signals in target directions orthogonal to each other. Taking the case of two targets as an example, we can obtain the baseband transmit waveform of the m-th antenna as

$$g_o[n] = \begin{bmatrix} \widetilde{x}_m(\theta_1, n) & \widetilde{x}_m(\theta_2, n) & \widetilde{x}_m(\theta_1, n) & -\widetilde{x}_m(\theta_2, n) \end{bmatrix} \tag{32}$$

Assuming the number of MIMO radar antennas is $M = 8$ and targets are located in directions $\theta_1 = -20^\circ, \theta_2 = 20^\circ$, the transmit waveform of the 5th channel generated by the above method is shown in Figure 7. In Figure 7b, discrete frequency spectrum components of different colors correspond to the signals in Figure 7a, which will be transmitted in different directions after beamforming. Under a small time-bandwidth product, the frequency spectrum of the LFM signal calculated by the principle of stationary phase is not flat. Therefore, amplitudes of the two targets are not the same.



(**a**) (**b**)

Figure 7. The transmit waveform of the 5th channel. (**a**) Time domain (real part); (**b**) frequency domain.

The 2D orthogonal waveform generation for multi-target ISAR imaging can be divided into the following steps, and the flowchart is shown in Figure 8.

Step 1: Get the azimuth information $[\theta_1, \theta_2, \cdots, \theta_H]$ and time duration T_h.

Step 2: After time-variant weighting, each transmit waveform $\widetilde{x}_m(\theta_h, t)$ can form a single beam pointing in the target direction.

Step 3: Zero fills each signal $\widetilde{x}_m(\theta_h, t)$ to the same length N and ensures that the signal parts do not overlap in time.

Step 4: After OFDM chirp modulation, each transmit waveform $g_h[n]$ will form a single beam, and synthetic signals in each beam direction are approximately orthogonal.

Step 5: The sum of multiple transmit waveforms can still maintain constant modulus characteristics.

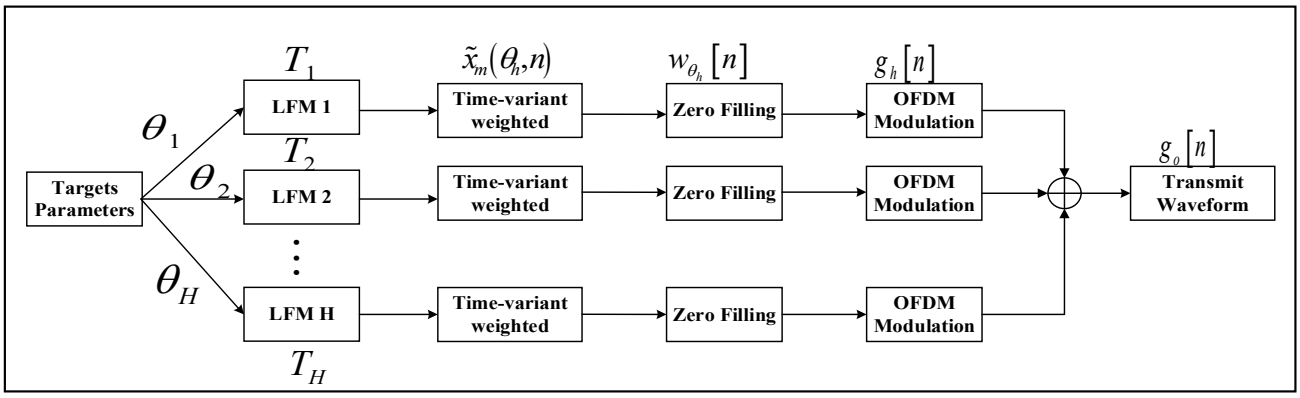


Figure 8. The flowchart of the proposed method.

4.3. Analysis of the Proposed Method for Multi-Target Imaging

In the previous section, we gave a method to obtain 2D orthogonal waveforms for multi-target ISAR imaging with OFDM modulation. Here, we are going to conduct a systematic analysis of the proposed method.

A. Time Complexity

Obviously, the proposed method directly generates the transmit waveforms, which is different from the non-convex optimization method mentioned in Section 3.2. Typically, the latter has iterative optimization processes, resulting in a significant time overhead. In Table 1, we summarize the time complexity of several existing waveform design algorithms that can be used for multi-target imaging.

Table 1. The time complexity.

Algorithms	Time Complexity
This paper	$O(HMN)$
CG algorithm in paper [21]	$O\left(I_1 KMN^2\right)$
IOA algorithm in paper [22]	$O\left(I_2 (MN)^2\right)$
IOA algorithm in paper [23]	$O(I_3 MN(N + \log_2 N))$

I_1, I_2, I_3 are the required total iteration numbers of the above algorithms. M is the number of emitting antennas. N is the length of the discrete baseband signal. H is the number of targets. K is the discrete azimuth number. It can be seen that this algorithm has less time overhead, and the gap between the above methods will rapidly increase with the increase in iteration times and signal length.

B. Constraints of the Proposed Method

The proposed method designs the phase of the baseband transmit waveform, similar to the phase-encoded signal. In this paper, we assume that each radar element can generate arbitrary waveform signals independently, which a newly full DAR can achieve.

For moving aerospace targets, their echoes have Doppler frequency shifts, which will weaken the orthogonality of signals proposed in Formula (5). Therefore, this algorithm is only applicable to low-speed targets.

Based on OFDM modulation, we can only obtain orthogonal imaging signals with uniformly distributed discrete frequency spectrum, resulting in grating lobes in the results of pulse compression. As the number of targets increases, the spacing between the main lobe and the grating lobe will become narrower, which may lead to one-dimensional range profile aliasing.

5. Experiments and Results

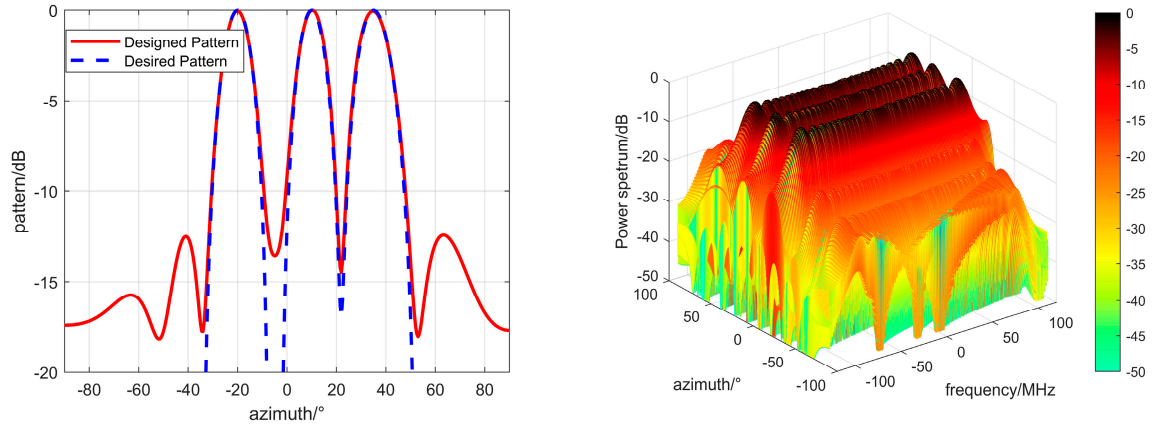
5.1. Validation of Transmit Waveform for Multi-Target Imaging

We consider a co-located MIMO radar system with M transmit antennas, which are deployed as a ULA with inter-element spacing of $d = c/2(f_c + B/2)$. And the simulation parameters of the MIMO radar are shown in Table 2.

Table 2. The simulation parameters of the MIMO radar.

Parameters	Value
Number of antennas M	10
Carrier frequency f_c	1 GHz
Signal bandwidth B	200 MHz
Sampling frequency F_s	240 MHz
Pulse Duration T_p	6 μs
Discrete azimuth number K	361
Target number	3
Target azimuth	$[-20^\circ, 10^\circ, 35^\circ]$

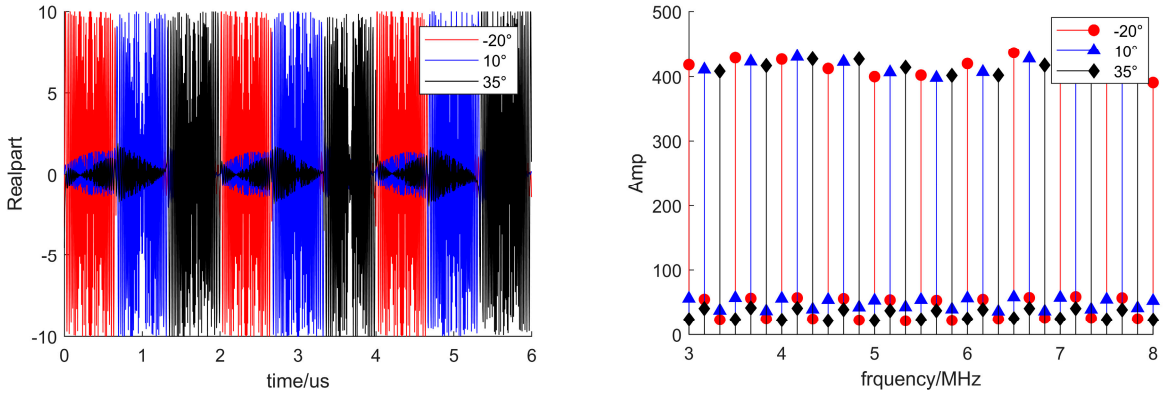
According to the proposed algorithm, we can obtain a transmit waveform, and the beampattern is shown in Figure 9a. It forms three beams pointing in the directions -20°, 10° and 35° simultaneously. Also, the actual pattern approximates the desired pattern, which is given by the traditional narrowband PAR beamforming algorithm. The discrete power spectrum of the designed waveform in the 2D space–frequency joint domain is shown in Figure 9b. It can be clearly seen that the synthetic signals in directions -20°, 10° and 35° cover the same frequency band.



(**a**) (**b**)

Figure 9. The beampattern and discrete power spectrum of simulation. (**a**) Beampattern; (**b**) discrete power spectrum in space–frequency 2D joint domain.

In addition, synthetic signals in directions −20°, 10° and 35° are shown in Figure 10, which are similar to chirp signals. However, the main part of the synthetic signals does not overlap in the time domain. It is worth noting that we cannot obtain three completely orthogonal detection signals due to the sidelobe effect of beamforming. Therefore, discrete frequency components of different synthetic signals are only approximately non-overlapping. Define the discrete frequency component with amplitude close to the maximum as the effective part of the target echo.



(**a**) (**b**)

Figure 10. The synthetic signals in directions −20°, 10° and 35°. (**a**) Time domain (real part); (**b**) frequency domain.

Assuming that three ideal scattering points are located at the same distance and in different directions, the mixed echo from them is approximated in Figure 10a. However, we cannot separate the mixed echo by time domain windowing because of different target distances in real scenes. In this paper, we used matched filters to separate the mixed echo at the receiving end, and this process is realized in the frequency domain. Matched filters 1–3 are the complex conjugate of the frequency spectrum of synthetic signals in target directions. After matched filtering, the pulse compression results are shown in Figure 11. It can be seen that echoes from different targets can only obtain high-peak amplitude with the corresponding matched filter. When the target echoes do not correspond to the filter, the results will show a low-peak amplitude, which can be seen as a suppression of these echoes. In addition, we analyze the separation of multi-target echo and compare it with the conventional method based on spatial filtering at the receiver. Numerical results are shown in Table 3.

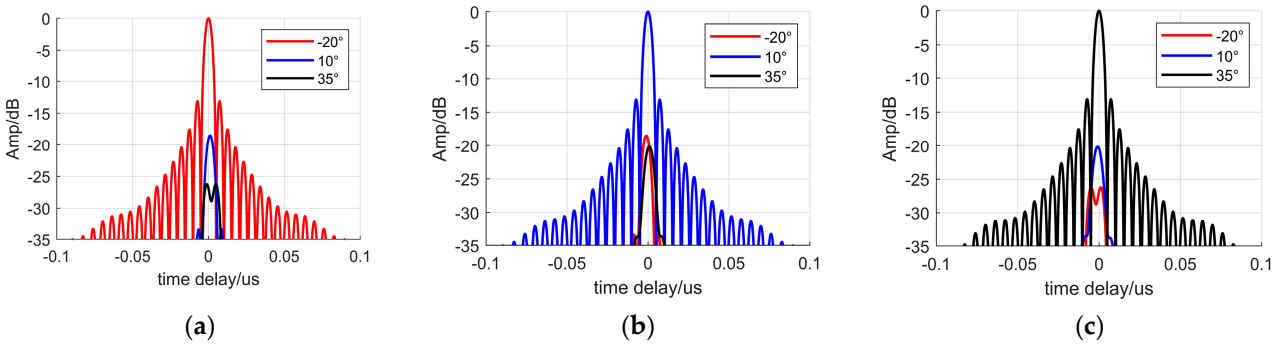


Figure 11. The results of pulse compression. (**a**) Matched filter 1; (**b**) matched filter 2; (**c**) matched filter 3.

Table 3. The separation of multi-target echoes.

Mixed Echo	Separation in This Paper (dB)	Separation in Paper [23] (dB)	Separation in Spatial Filtering (dB)
−20° and 10°	−18.5	−18.4	−17.6
10° and 35°	−20.2	−20.8	−19.9
−20° and 35°	−26.7	−26.9	−25.9

Set targets in each beam direction and conduct echo simulation using the ISAR imaging model. Scattering models of targets are shown in Figure 12a–c. The imaging results of mixed echo after matched filtering, translation compensation and keystone transformation are shown in Figure 12d–f.

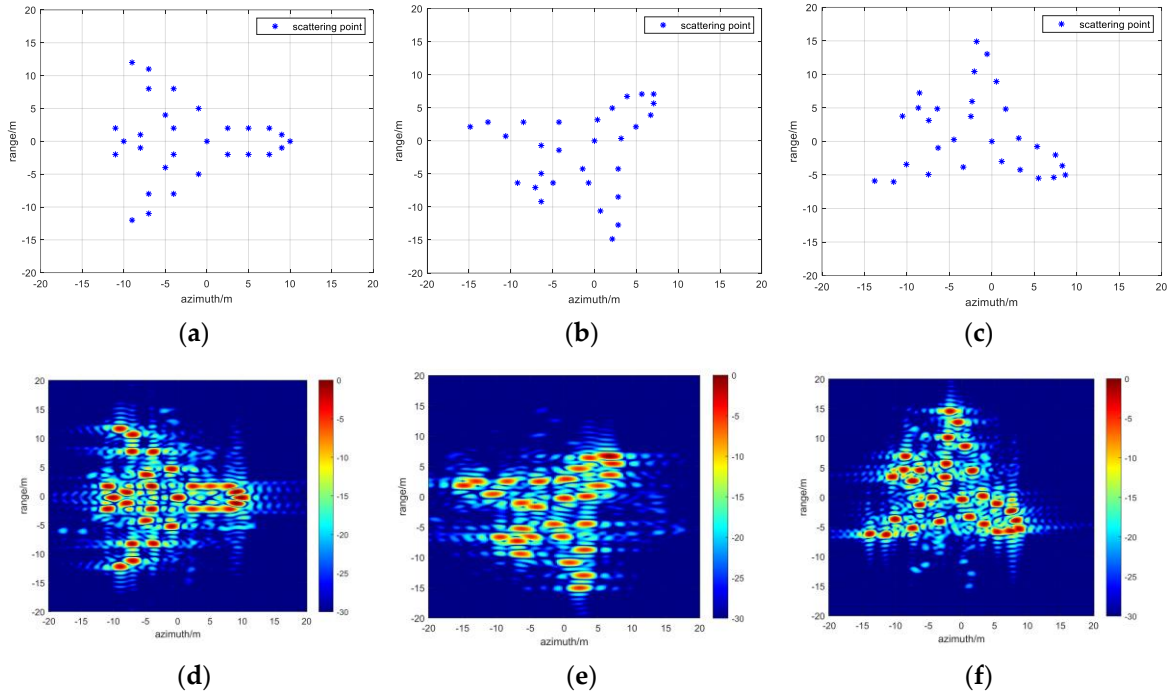


Figure 12. Simulation results of multi-target ISAR imaging. (**a**) Scattering model 1; (**b**) scattering model 2; (**c**) scattering model 3; (**d**) imaging result of target 1; (**e**) imaging result of target 2; (**f**) imaging result of target 3.

The algorithm proposed in the paper [23] can also achieve similar functions. Under the same hardware conditions, we further calculated the time overhead to generate the

transmit waveform, and the results are shown in Table 4. The data show that as the length of the transmit waveform increases, the time overhead required by the algorithm proposed in this paper slowly increases. With the signal length increasing, more unknown parameters need to be optimized, resulting in significant time overhead in the paper [23].

Table 4. The time overhead of waveform design.

Signal Length (μs)	Time Overhead in Paper [23] (s)	Time Overhead in This Paper (s)
4	0.721	0.0167
8	4.108	0.0175
12	13.141	0.0178
16	43.209	0.0186

5.2. Experimental Verification of the Proposed Algorithm

In this section, we used a newly full DAR to validate the proposed algorithm. This equipment is shown in Figure 13.



(**a**) (**b**)

Figure 13. The equipment used for outdoor experiment. (**a**) DAR radar; (**b**) corner reflector.

This radar has eight transmit antennas and eight receive antennas. Each antenna can be independently controlled, allowing the transmit waveform to be arbitrarily designed. Based on this equipment, we set the system parameters as shown in Table 5 and carried out outdoor experiments.

Table 5. The system parameters of the MIMO radar.

Parameters	Value
Number of antennas M	4
Carrier frequency f_c	17 GHz
Signal bandwidth B	40 MHz
Signal duration T_p	10 μs
Sampling frequency F_s	80 MHz
Element spacing d	60 mm
Pulse repetition frequency (PRF)	1000 Hz
Target azimuth	$[-4°, 4°]$

To verify the effectiveness of the designed transmit waveform, we designed the following experimental scene, as shown in Figure 14. The actual outdoor experimental site is a basketball court, with multiple corner reflectors placed on the ground as point targets. Therefore, there is interference clutter reflected from the ground, basketball stands, or trees

in the mixed echo. Although most background noise can be removed by subtraction and cancellation, some random signals still affect the experimental results. For this reason, there may be inconsistencies in the subsequent analysis of the results.

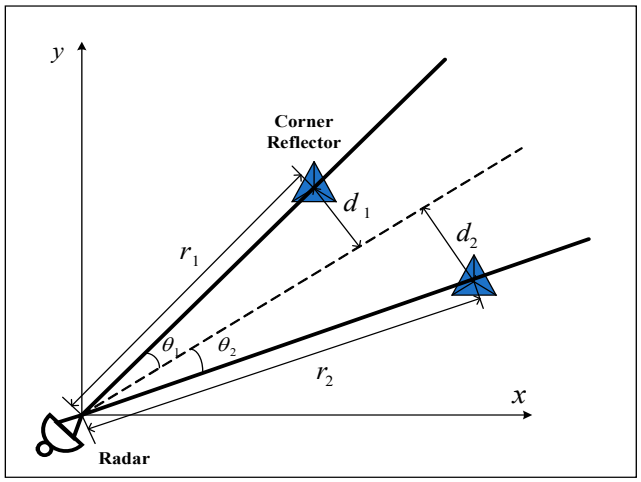
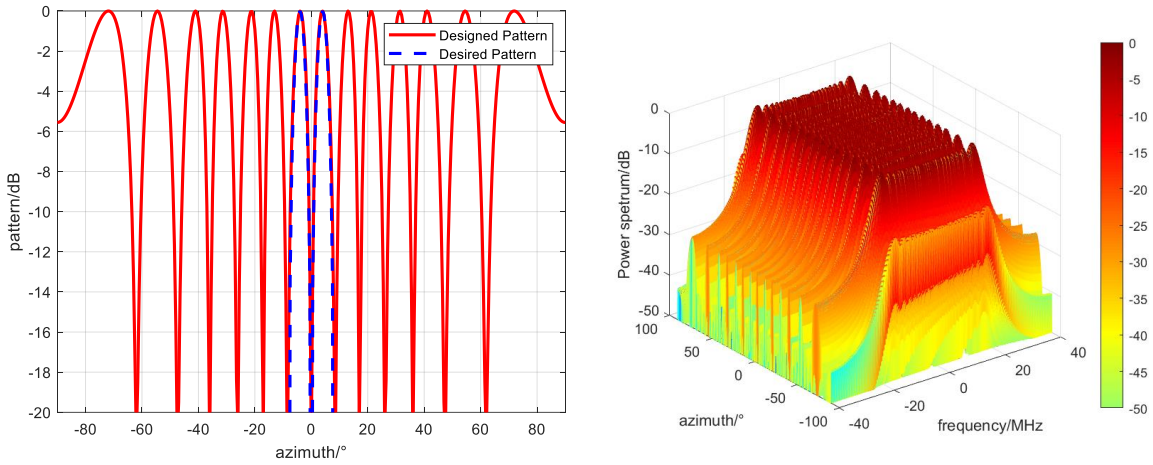


Figure 14. The experimental scene.

The distance between the corner reflector and the radar in Figure 14 should meet the far-field condition. In this experiment, the distance should be further than 26 m. In addition, due to the element spacing d being longer than the half-wavelength $\lambda/2$, there are many grating lobes in the beampattern. Therefore, the target azimuth interval should be less than the unambiguous range to avoid the influence of grating lobes. Set the targets in directions $-4°$ and $4°$, and the beampattern and discrete power spectrum are shown in Figure 15.

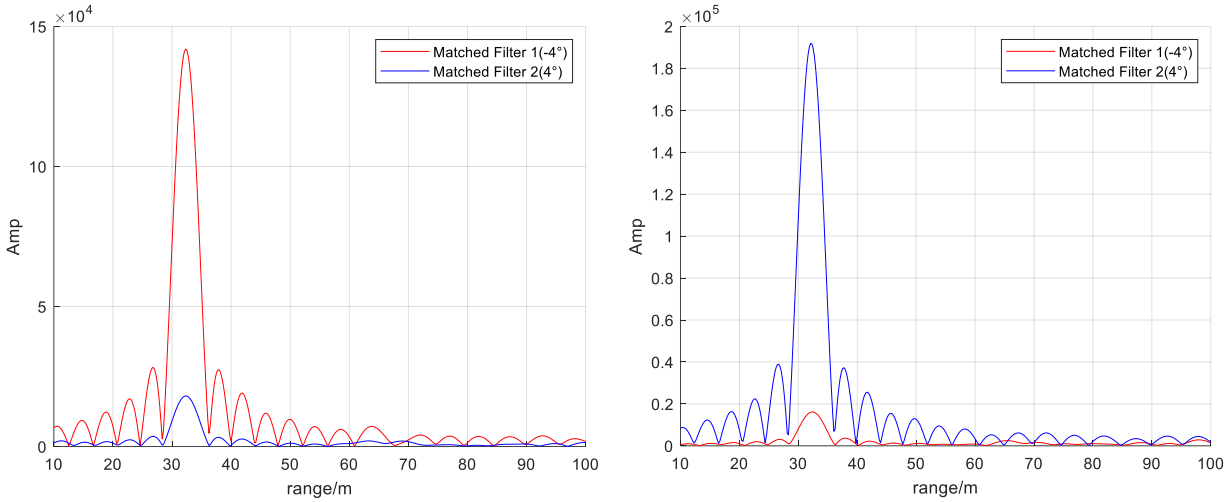


(**a**) (**b**)

Figure 15. The beampattern and discrete power spectrum of experiment. (**a**) Beampattern; (**b**) discrete power spectrum in space–frequency 2D joint domain.

Assuming that a corner reflector is placed sequentially at the polar coordinates $(-4°$, 32 m) and $(4°$, 32 m), the synthetic signals in these directions are reflected by targets and received by the radar. For an echo from a single target after pre-processing and matched filtering with its corresponding filter, we can observe the target with a high peak value, as shown in Figure 16. However, when using a non-corresponding filter to process the echo, the target will have a very low amplitude or even be submerged in noise. Figure 16a shows the pulse compression result of the echo from the target in the direction $-4°$, while

Figure 16b shows the target in the direction 4°. Both of them use the same matched filters. Therefore, when we determine the matched filter, we will only observe one target in the one-dimension range profile.

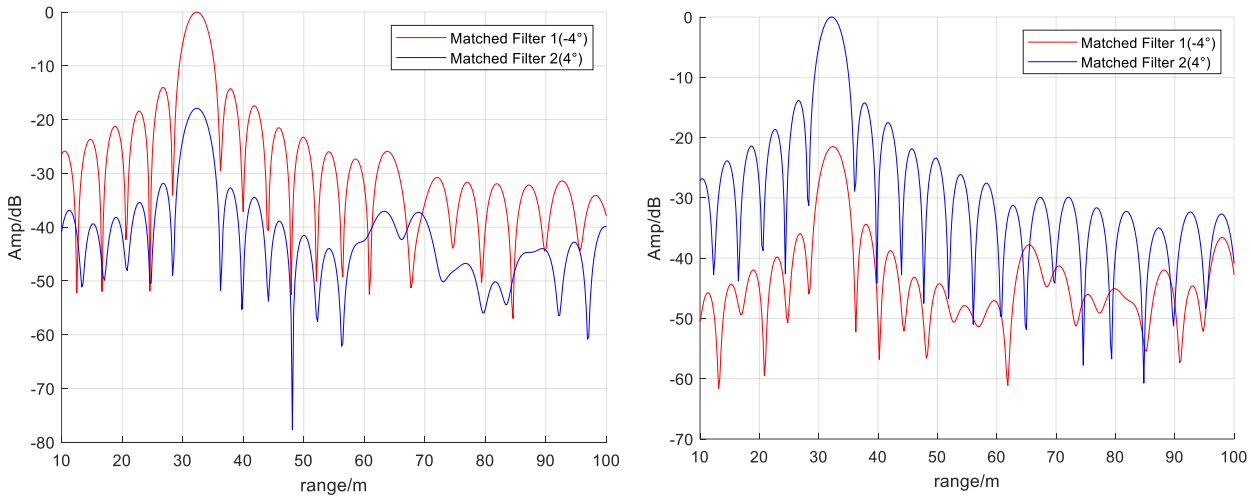


(**a**) (**b**)

Figure 16. Pulse compression result of the target echo. (**a**) −4°; (**b**) 4°.

Since the targets are not precisely aligned with the beam directions, the corresponding antenna gain for targets will be slightly different, which makes the amplitudes of the two target echoes different. Moreover, this factor will also affect the orthogonality of the target echoes.

The logarithmic form of the above data is shown in Figure 17. As aforementioned, the pulse compression result will be relatively reduced by about 17.9 dB for the target in the direction −4° when using a non-corresponding filter. And this value is about 21.5 dB for the target in the direction 4°. The peak sidelobe level for both data is about −14 dB, similar to the ideal LFM waveform.

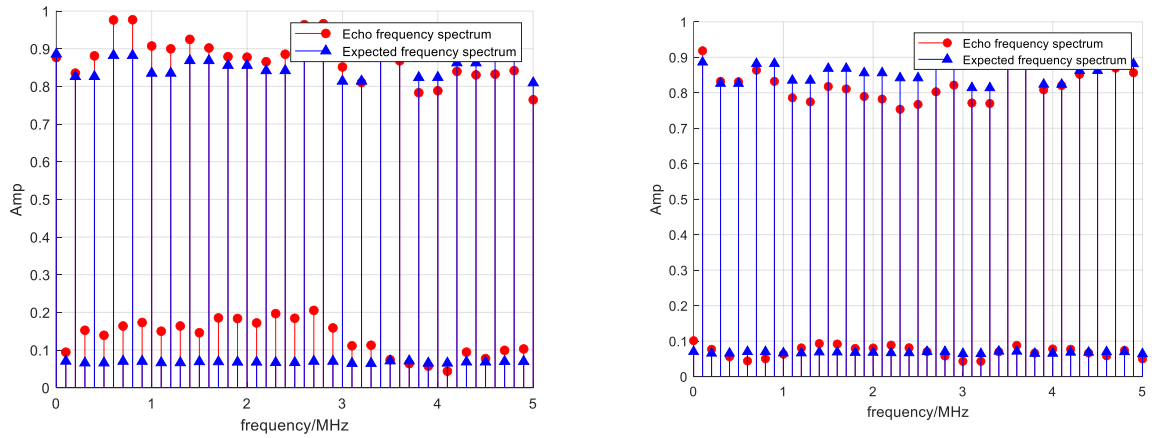


(**a**) (**b**)

Figure 17. One dimensional range profile of the target echo (dB). (**a**) −4°; (**b**) 4°.

Using the fast Fourier transform (FFT) to analyze the echoes and normalized discrete frequency spectra are shown in Figure 18. In Figure 18a, most of the echo energy from target1 occupies the odd frequency points. And in Figure 18b, even frequency points are

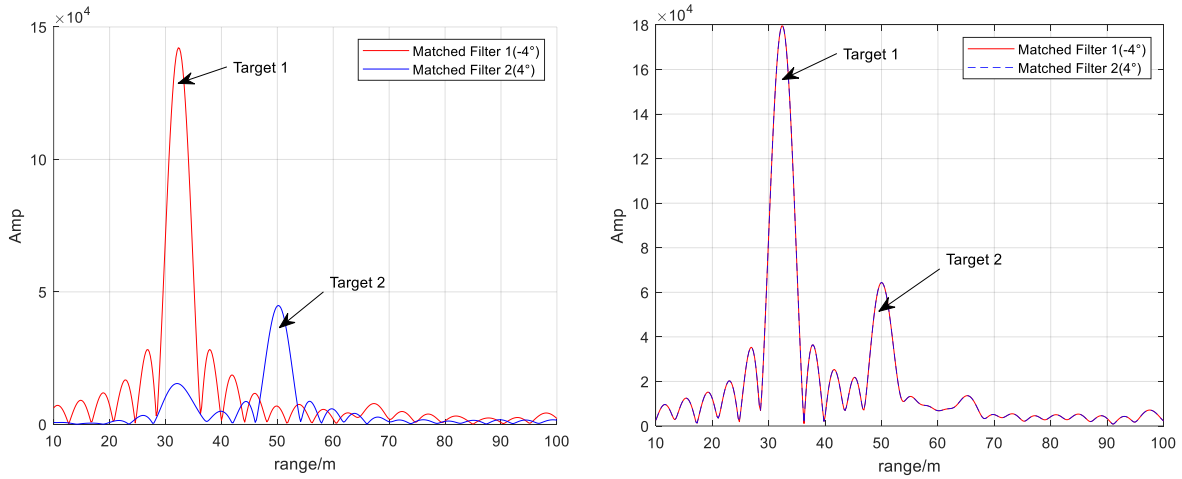
occupied. It can be seen that we have indeed synthesized approximately orthogonal signals similar to the OFDM chirp theory in target directions. The expected frequency spectrum is given by the proposed algorithm in this paper. In addition, background clutter will also cause some interference with the spectrum analysis. Therefore, the amplitude of some discrete frequency points will deviate from the expected value.



(**a**) (**b**)

Figure 18. The discrete frequency spectrum of the target echo (dB). (**a**) −4°; (**b**) 4°.

Next, we placed two targets at polar coordinates (−4°, 32 m) and (4°, 50 m). The echo data obtained are processed and shown in Figure 19. Two transmit waveforms are used for target detection, and all targets can be distinguished well. In Figure 19a, we can see the suppression effect of different matched filters on the targets. In Figure 19b, we use the ideal LFM waveform to form multiple beams, and each target is detected by the same signal. Therefore, multiple targets cannot be observed independently. The difference in amplitude between different targets is related to their distance. The difference in amplitude of the same target between the above waveforms is because we only use data within the valid discrete frequency component for processing in Figure 19a.



(**a**) (**b**)

Figure 19. Pulse compression results under different transmit waveform. (**a**) The waveform proposed in this paper; (**b**) LFM waveform.

6. Conclusions

This paper proposes a novel waveform design method based on beam-waveform 2D orthogonality for multi-target imaging. With the OFDM modulation theory, we can

directly generate the constant modulus transmit waveform, which can image different targets with approximately orthogonal signals. Simulation and experimental results show that the algorithm has a lower time complexity than the traditional algorithm and realizes mixed echo separation by matched filtering, thus improving the radar working efficiency significantly. In the future, we plan to consider the target's prior information to improve the applicability of the proposed algorithm.

Author Contributions: All of the authors made significant contributions to the work. X.Z. and G.J. provided the research ideals. X.Z. completed simulation experiments and wrote the manuscript; G.J., F.H. and Y.Z. provided insightful suggestions for the work and the manuscript. All authors have read and agreed to the published version of the manuscript.

Funding: This research received no external funding.

Data Availability Statement: The data presented in this study are available on request from the corresponding author.

Acknowledgments: The authors would like to thank all the anonymous reviewers for their valuable comments and helpful suggestions, which led to substantial improvements of this paper.

Conflicts of Interest: The authors declare no conflicts of interest.

References

1. Lee, H.-S.; Shin, B.-S.; Thomasson, J.A.; Wang, T.; Zhang, Z.; Han, X. Development of Multiple UAV Collaborative Driving Systems for Improving Field Phenotyping. *Sensors* **2022**, *22*, 1423. [CrossRef]
2. Ding, H.; Zhang, S.; Gong, F.; Wang, W.; Tian, H. Imaging of Moving Target for Cooperative Sar Between High-Orbit and Low-Orbit Satellites. In Proceedings of the IGARSS 2018—2018 IEEE International Geoscience and Remote Sensing Symposium, Valencia, Spain, 22–27 July 2018; pp. 597–600. [CrossRef]
3. Zheng, H.; Jiu, B.; Liu, H. Waveform Design Based ECCM Scheme Against Interrupted Sampling Repeater Jamming for Wideband MIMO Radar in Multiple Targets Scenario. *IEEE Sens. J.* **2022**, *22*, 1652–1669. [CrossRef]
4. Zhu, J.; Song, Y.; Jiang, N.; Xie, Z.; Fan, C.; Huang, X. Enhanced Doppler Resolution and Sidelobe Suppression Performance for Golay Complementary Waveforms. *Remote Sens.* **2023**, *15*, 2452. [CrossRef]
5. Raei, E.; Alaee-Kerahroodi, M.; Babu, P.; Bhavani Shankar, M.R. Generalized waveform design for sidelobe reduction in MIMO radar systems. *Signal Process.* **2023**, *206*, 108914. [CrossRef]
6. Chen, J.; Xiao, H.; Song, Z.; Fan, H. Simultaneous ISAR imaging of group targets flying in formation. *Chin. J. Aeronaut.* **2014**, *27*, 1554–1561. [CrossRef]
7. Chen, V.C.; Qian, S. Joint time-frequency transform for radar range-Doppler imaging. *IEEE Trans. Aerosp. Electron. Syst.* **1998**, *34*, 486. [CrossRef]
8. Kong, L.; Zhang, W.; Zhang, S.; Zhou, B. Radon transform and the modified envelope correlation method for ISAR imaging of multi-target. In Proceedings of the 2010 IEEE Radar Conference, Arlington, VA, USA, 10–14 May 2010; pp. 637–641.
9. Xueru, B.; Feng, Z.; Mengdao, X.; Zheng, B. A Novel Method for Imaging of Group Targets Moving in a Formation. *IEEE Trans. Geosci. Remote Sens.* **2012**, *50*, 221–231. [CrossRef]
10. Xiao, D.; Su, F.; Wu, J. Multi-target ISAR imaging based on image segmentation and Short-time Fourier Transform. In Proceedings of the 2012 5th International Congress on Image and Signal Processing, Chongqing, China, 16–18 October 2012; pp. 1832–1836. [CrossRef]
11. Liu, L.; Zhou, F.; Tao, M.; Zhang, Z. A Novel Method for Multi-Targets ISAR Imaging Based on Particle Swarm Optimization and Modified CLEAN Technique. *IEEE Sens. J.* **2016**, *16*, 97–108. [CrossRef]
12. Li, H.; Su, F. A Multi-Target ISAR Imaging Method Based on Zhang-Suen Thinning and Radon Transform. In Proceedings of the 2022 15th International Congress on Image and Signal Processing, BioMedical Engineering and Informatics (CISP-BMEI), Beijing, China, 5–7 November 2022; pp. 1–5.
13. Zhang, Y.; Xu, N.; Li, N.; Guo, Z. A Multi-Domain Joint Novel Method for ISAR Imaging of Multi-Ship Targets. *Remote Sens.* **2023**, *15*, 4878. [CrossRef]
14. Li, Y.; Wang, J.; Liu, R.; Ding, J.; Zhang, P.; Xing, M. Joint Translational Motion Compensation for Multitarget ISAR Imaging Based on Integrated Kalman Filter. *IEEE Trans. Geosci. Remote Sens.* **2023**, *61*, 5108716. [CrossRef]
15. Li, G.; Hou, Q.; Xu, S.; Chen, Z. Multi-target simultaneous ISAR imaging based on compressed sensing. *EURASIP J. Adv. Signal Process.* **2016**, *2016*, 27. [CrossRef]
16. Chen, Y.; Zhang, Q.; Yuan, N.; Luo, Y.; Lou, H. An Adaptive ISAR-Imaging-Considered Task Scheduling Algorithm for Multi-Function Phased Array Radars. *IEEE Trans. Signal Process.* **2015**, *63*, 5096–5110. [CrossRef]
17. Stoica, P.; Jian, L.; Yao, X. On Probing Signal Design for MIMO Radar. *IEEE Trans. Signal Process.* **2007**, *55*, 4151–4161. [CrossRef]

18. Stoica, P.; Li, J.; Zhu, X. Waveform Synthesis for Diversity-Based Transmit Beampattern Design. *IEEE Trans. Signal Process.* **2008**, *56*, 2593–2598. [CrossRef]
19. Zheng, H.; Jiu, B.; Li, K.; Liu, H. Joint Design of the Transmit Beampattern and Angular Waveform for Colocated MIMO Radar under a Constant Modulus Constraint. *Remote Sens.* **2021**, *13*, 3392. [CrossRef]
20. He, H.; Stoica, P.; Li, J. Wideband MIMO Systems: Signal Design for Transmit Beampattern Synthesis. *IEEE Trans. Signal Process.* **2011**, *59*, 618–628. [CrossRef]
21. Liu, H.; Wang, X.; Jiu, B.; Yan, J.; Wu, M.; Bao, Z. Wideband MIMO Radar Waveform Design for Multiple Target Imaging. *IEEE Sens. J.* **2016**, *16*, 8545–8556. [CrossRef]
22. Yu, X.; Cui, G.; Yang, J.; Kong, L. Wideband MIMO radar beampattern shaping with space-frequency nulling. *Signal Process.* **2019**, *160*, 80–87. [CrossRef]
23. Zou, X.; Jin, G.; He, F.; Zhang, Y. A Novel MIMO Radar Waveform Design Method for Multi-Target ISAR Imaging. In Proceedings of the 2023 6th International Conference on Electronics Technology (ICET), Chengdu, China, 12–15 May 2023; pp. 1371–1375. [CrossRef]
24. Chu, C.; Chen, Y.; Luo, Y.; Zhang, Q. Wideband MIMO Radar Waveform Design Under Multiple Criteria. *IEEE Geosci. Remote Sens. Lett.* **2023**, *20*, 3298098. [CrossRef]
25. Chen, Y.J.; Zhang, Q.; Luo, Y.; Li, K.M. Multi-Target Radar Imaging Based on Phased-MIMO Technique—Part II: Adaptive Resource Allocation. *IEEE Sens. J.* **2017**, *17*, 6198–6209. [CrossRef]
26. Zhang, M.; Liao, G.; Xu, J.; Lan, L.; Deng, K. ISAR Imaging of Multiple Targets with Time-Delay Receive Array. *IEEE Access* **2020**, *8*, 199759–199767. [CrossRef]
27. Wang, D.; Zhang, Q.; Luo, Y.; Li, K.M.; Liu, X.W. Task Scheduling for Multi-Target ISAR Imaging in Radar Network. *IEEE Access* **2020**, *8*, 46092–46101. [CrossRef]
28. Wang, D.; Zhang, Q.; Luo, Y.; Liu, X.; Ni, J.; Su, L. Joint Optimization of Time and Aperture Resource Allocation Strategy for Multi-Target ISAR Imaging in Radar Sensor Network. *IEEE Sens. J.* **2021**, *21*, 19570–19581. [CrossRef]
29. Liu, X.W.; Zhang, Q.; Luo, Y.; Chen, Y.J.; Lu, X. ISAR Imaging Task Allocation for Multi-Target in Radar Network Based on Potential Game. *IEEE Sens. J.* **2019**, *19*, 11192–11204. [CrossRef]
30. Kim, J.H.; Younis, M.; Moreira, A.; Wiesbeck, W. A Novel OFDM Chirp Waveform Scheme for Use of Multiple Transmitters in SAR. *IEEE Geosci. Remote Sens. Lett.* **2013**, *10*, 568–572. [CrossRef]

Disclaimer/Publisher's Note: The statements, opinions and data contained in all publications are solely those of the individual author(s) and contributor(s) and not of MDPI and/or the editor(s). MDPI and/or the editor(s) disclaim responsibility for any injury to people or property resulting from any ideas, methods, instructions or products referred to in the content.